AIAA JOURNAL
Vol. 35, No. 1, January 1997

Airfoil Boundary-Layer Development and Transition with Large Leading-Edge Roughness

Michael F. Kerho* and Michael B. Bragg†
University of Illinois at Urbana–Champaign, Urbana, Illinois 61801-2935

An experimental study of the effects of large distributed roughness located near the leading edge of an airfoil has been performed to determine the effect on boundary-layer development and transition. Boundary-layer measurements were carried out on a two-dimensional NACA 0012 airfoil with a 53.34-cm chord through the use of hot-wire anemometry at Reynolds numbers of 0.75×10^6, 1.25×10^6, and 2.25×10^6. These measurements included mean and fluctuating velocity, turbulence intensity, flowfield intermittency, and associated integral parameters. The roughness used was of the type and density observed to occur during the initial glaze ice accretion process. Results have shown that the transitional boundary layer induced by large distributed roughness is markedly different from the smooth model Tollmein–Schlicting induced transition process. No fully developed turbulent boundary layers were observed to occur near the roughness location. Instead, the large distributed roughness was observed to trigger a transitional boundary layer at or very near the roughness location. This transitional boundary layer required a substantial chordwise extent to obtain a fully developed turbulent state. Streamwise turbulence intensity levels in the roughness induced transitional region were observed to be relatively low as compared with the smooth model transitional region.

Nomenclature

C_p = pressure coefficient, $(p - p_\infty)/(0.5\rho U_\infty^2)$
c = model chord length
k = roughness height
R = specific gas constant
Re = Reynolds number based on chord, $(\rho U_\infty c)/\mu$
Re_k = roughness Reynolds number based on height k, $(\rho U_k k)/\mu$
$Re_{k,\,\mathrm{crit}}$ = critical roughness Reynolds number
Re_x = running Reynolds number based on surface length, $(\rho U_\infty s)/\mu$
s = surface length from the stagnation point
T = total sampling time
U_k = undisturbed velocity at the roughness height
U_∞ = freestream velocity
u = streamwise velocity component
u' = streamwise perturbation velocity component
$\hat{u}'$ = integrated turbulence intensity normalized by airfoil chord
u'_{rms} = turbulence intensity, given in percent freestream
x = streamwise coordinate
y = coordinate normal to the model chord
z = distance normal to the model surface
α = model angle of attack
γ = intermittency
$\hat{\gamma}$ = integrated intermittency normalized by the boundary-layer thickness
$\Delta x_{tr}/c$ = nondimensional chordwise extent of the transitional zone
δ = boundary-layer thickness
Θ = boundary-layer momentum thickness
μ = viscosity
ρ = ambient air density

Received March 27, 1995; revision received Sept. 19, 1996; accepted for publication Sept. 26, 1996; also published in *AIAA Journal on Disc*, Volume 2, Number 2.

*Graduate Research Associate, Department of Aeronautical and Astronautical Engineering, 306 Talbot Laboratory, 104 South Wright Street; currently Senior Engineer/Scientist, McDonnell Douglas Aerospace, Mail Code 71-35, Long Beach, CA 90810. Member AIAA.

†Professor, Department of Aeronautical and Astronautical Engineering, 306 Talbot Laboratory, 104 South Wright Street. Associate Fellow AIAA.

Introduction

THE study of the aerodynamic effect of surface roughness and surface contamination has been an important and active field of research for the last 60 years. Over this period, significant advances have been made in understanding the effect surface roughness has upon a given flowfield. Unfortunately, the underlying physical processes are so complex and nonlinear that they make analytical and even computational description extremely difficult if not impossible at this time. As a result, the majority of engineering work with surface roughness has been to develop empirical relationships in an attempt to include roughness effects in the analysis of fluid mechanics problems. Scientific studies have also been conducted in an attempt to understand the mechanisms by which roughness affects the boundary layer and surrounding flowfield. Although both the engineering and scientific communities have produced significant results, neither has been able to completely understand or effectively deal with the problem of surface roughness. A current area of research dominated by leading-edge surface roughness effects is the problem of ice accretion on airfoil and aircraft surfaces.

It is known that small surface roughness primarily causes premature boundary-layer transition. Traditionally there have been two avenues of roughness research: those researchers concerned with size and location of roughness and its effect upon airfoil transition location and performance and those researchers concerned with the fluid dynamic mechanisms by which roughness affects the boundary layer and surrounding flowfield. As a result, previous experimental studies of roughness have either been to document the transition location and resulting performance degradation on an airfoil as a function of roughness size and placement or to study the instability mechanisms generated by roughness that cause premature transition. The latter set of experiments on roughness transition mechanisms have been conducted almost solely on a flat plate with zero pressure gradient. For both types of research, the majority of analysis has been performed for roughness heights smaller than the boundary-layer thickness.

Very few data exist for large roughness located in the leading-edge region of an airfoil. The goal of the research performed for this study is to provide a detailed analysis of the boundary-layer development as a result of large distributed roughness typical of that present during the early ice accretion process in the leading-edge stagnation region of an airfoil. The results are directly applicable to the ice accretion modeling process and will help to provide detailed insight into the driving mechanisms affecting the early accretion process. Results should also prove useful to those interested in large-scale

leading-edge roughness effects and the ensuing transitional boundary layer.

Boundary-Layer Transition

For a smooth airfoil at low Mach number, transition of the boundary layer usually occurs as a result of the development of Tollmein–Schlichting (TS) waves. These linear waves breakdown into nonlinear three-dimensional instabilities and finally form turbulent spots that coalesce to form a turbulent boundary layer. This process takes a finite distance to develop from the initial growth of the TS waves to a fully developed turbulent boundary layer. The introduction of surface roughness into the preceding processes can greatly enhance certain growth regimes or bypass others altogether.

There are three types of simulated roughness generally considered: a two-dimensional isolated roughness such as a spanwise two-dimensional trip, an isolated three-dimensional element such as a hemisphere or circular cylinder, and distributed roughness that can include grit or large numbers of densely packed hemispheres or cylinders. The effects of roughness are dependent upon its relative height in the boundary layer. Usually roughness heights are nondimensionalized by the displacement thickness $k/\delta*$ or a roughness Reynolds number Re_k.

Beginning with the early work of Gregory and Walker,[1] the subcritical flow about a single isolated hemisphere in a laminar boundary layer is well documented. At $Re_k = 300$, before the element promotes early boundary-layer transition, the dominant feature of the flowfield is that of a primary horseshoe vortex generated due to boundary-layer separation on the wall at the element leading edge. Smaller secondary and tertiary vortices have also been observed. Aft of the element a pocket of separated flow is observed with a pair of spiral vortices that take mass up away from the wall and trail downstream rotating in the opposite sense from the horseshoe vortices.

At a higher Re_k (350–450) the shear layer of the top of the element becomes unstable and hairpin vortices are shed.[2] It is not clear whether this is related to the spiral vortices or a completely different mechanism. The shedding frequency is above that for TS instabilities. If Re_k is increased further, boundary-layer transition occurs in a wedge of turbulent flow (turbulent wedge) downstream of the element. The exact transition mechanism is unknown but is thought to be related to instabilities in the element's vortex structure. This type of transition bypasses known linear transition processes and is referred to as bypass transition.[3]

For the case of distributed roughness the flowfield is not as well understood. Kendall[4] measured velocity profiles downstream of distributed roughness and noted the outward movement of the velocity profile due to the element blockage. Kendall also documented the presence of an inflectional velocity profile. Corke et al.[5] found that the highest peaks in a distributed roughness do not cause an isolated wedge-type transition. Neither TS transition nor inflectional boundary-layer profiles were observed, but there was evidence of three-dimensional flow unsteadiness at higher Re_k. Tadjfar et al.[6] made detailed measurements around three-dimensional roughness elements. At $Re_k = 160$ no separation was observed about the elements, but at 3.5×10^2 separation and reverse flow was present behind an element. No TS waves were present, and inflectional profiles were measured. Tadjfar et al. speculated that the flowfield about individual elements were similar to the isolated case, except that the hairpin vortices were stronger than the horseshoe vortices.

Since bypass transition is a complex, nonlinear, and poorly understood process, no direct modeling or predictive capability exists at this time to predict roughness induced transition. Transition prediction is, therefore, almost exclusively done using empirical schemes based on the concept of a critical roughness Reynolds number $Re_{k,\,\mathrm{crit}}$. Studies on flat plates with small isolated roughness elements have shown that the origin of the turbulent wedge moves rapidly upstream and approaches the generating element with only a relatively small change in Re_k. The value of Re_k at which this occurs is usually referred to as the critical roughness Reynolds number. For roughness where the height of the element is less than the thickness of the laminar boundary layer, the flow about the element is well classified by Re_k.

Many researchers, using many different experimental techniques, have determined $Re_{k,\,\mathrm{crit}}$ values for isolated and distributed roughness. Early review articles on this topic include the work by Tani[7] and Von Deonhoff and Braslow.[8] Because of the wide difference in methods of determining $Re_{k,\,\mathrm{crit}}$ and different elements used and flowfields tested, the values vary significantly between researchers. Isolated element values typically range from 325 to 600 although values as high as 1000 have been reported. Distributed roughness $Re_{k,\,\mathrm{crit}}$ values of 600 are typical.

The results reported above, and almost all roughness data available in the literature, deal with roughness whose height is less than the local boundary-layer thickness and on a flat plate with no pressure gradient. However, in the icing case, the ice roughness is generally much larger than the boundary-layer thickness and on the airfoil leading edge where a large favorable pressure gradient exists. For distributed roughness, the critical roughness Reynolds number has been observed to be a function of Reynolds number based on distance from the leading edge Re_x. Braslow et al.[9] note that $Re_{k,\,\mathrm{crit}}$ increases from 600 to 1200 for distributed roughness for $Re_x < 150{,}000$. They speculated that this was due to the boundary-layer stability in a favorable pressure gradient and the effect of the roughness protruding out of the boundary layer. Bragg et al.[10] found isolated three-dimensional element $Re_{k,\,\mathrm{crit}}$ values exceeding 1700 on the leading edge of a NACA 0012 airfoil where the pressure gradient was large and $k/\delta > 3$. Norman[11] studied the flowfield about a roughness element when $k/\delta > 1$ in an attempt to better understand the transition mechanism. The large roughness element flowfield differed from the smaller roughness elements where $k/\delta < 1$ in terms of the unsteady flow about the element just before transition occurred. At a sufficiently high Re_k the horseshoe vortex system in front of the large roughness elements collapsed and reformed cyclically in a processes Norman referred to as burping. However, as before, the exact transition mechanism was not determined.

Summary

To date, most research dealing with distributed roughness has concentrated on small to moderate size roughness on a flat plate with zero pressure gradient. Measurements have dealt with the flowfield up until the point where an explosive nonlinear instability promotes premature transition. No instability mechanisms have been associated with this explosive breakdown.

Very little is known about the effect of large leading-edge distributed roughness where the size of the roughness is on the order of or greater than the local boundary-layer thickness. Roughness elements protruding through the boundary layer are more appropriately defined as obstacles having both viscous and inviscid dominated flow regions. The large size of the roughness is complicated by its leading-edge location in a favorable gradient. The present study documents the effect of this large distributed roughness on the development of an airfoil boundary layer. Detailed measurements in the transitional region downstream of the roughness are reported.

Experimental Procedure: Data Reduction and Error Analysis

The experimental equipment and procedures are discussed briefly in this section. A more detailed description is found in Kerho.[12]

These tests were conducted in the subsonic wind tunnel at the University of Illinois at Urbana–Champaign. The tunnel is of conventional design with approximately a 0.91×1.22 m test section. Test section speeds from 0 to 72 m/s are available at Reynolds numbers of up to 4.9×10^6/m. The tunnel is of open return type and uses four turbulence screens and honeycomb in the settling chamber to reduce tunnel turbulence to below 0.1%.

The NACA 0012 airfoil model used for this research is a two-dimensional model mounted vertically in the tunnel. The model had a span of 0.8573 m with a chord of 0.5334 m. The model was of a foam and fiberglass epoxy composite construction. All measurements reported in this paper were taken at a model angle of attack of zero degrees.

The distributed roughness was created by molding hemispherical shapes in staggered rows into strips of 0.5×4 in. plastic tape (see Fig. 1). To avoid confusion between the chordwise placement and extent of the distributed roughness, roughness chordwise extent will be reported in inches whereas chordwise placement from the stagnation point will be reported in millimeters. The roughness, including tape substrate, was nominally 0.35 mm high, and the roughness center to center spacing was 1.3 mm. The substrate

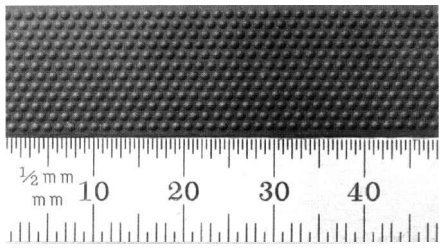

Fig. 1 Top view of the simulated distributed roughness.

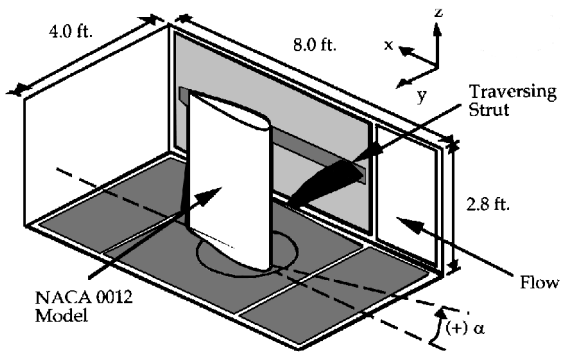

Fig. 2 Tunnel test schematic showing the NACA 0012 model in the test section.

thickness was 0.1 mm. The tape substrate was manufactured as thin as possible to minimize the leading- and trailing-edge step fore and aft of the simulated distributed roughness. Tests of the tape substrate thickness showed little to no effect upon the smooth model transition process. Smaller chordwise extents of the tape were obtained by cutting the 0.5-in. strips to obtain 0.25- and 0.125-in. extents.

The time-dependent boundary-layer velocity measurements were obtained using a single hot-wire probe. The wires used were platinum coated tungsten with diameters of 4 and 5 μm. The boundary-layer velocity profiles were obtained by traversing the probe normal to the local surface using a two-axis computer-controlled traverse. The traverse was used to position the probe with 0.01-mm resolution. The traverse system was completely contained in a pressure sealed box adjacent to the test section with the hot-wire probe mounted on a support arm extending from the traverse, through a streamwise slot and into the test section (see Fig. 2).

Output from the hot-wire anemometer was lowpass filtered at 1 kHz and acquired using an analog-to-digital conversion board contained in a 486-type personal computer. Measurements were taken using a 2-kHz sampling rate and 3000–4000 samples were acquired at each boundary-layer location. The data were digitally bandstop filtered from 160 to 225 Hz to remove probe vibration effects from the fluctuating signal. All hot-wire data were corrected for temperature and density variations. Turbulence intensity u_{rms}' was calculated from the velocity measurements using

$$u_{rms}'(\%) = \frac{100}{U_\infty}\left[\frac{1}{T}\int_0^T (u')^2\,\mathrm{d}t\right]^{\frac{1}{2}}$$

The hot-wire data were also processed to determine the flow intermittency. Intermittency is a measure of the amount of time the flow at a point in space is turbulent. The intermittency factor γ is defined to be 0.0 when the flow is fully laminar and 1.0 when the flow is fully turbulent. Intermittency was determined by digitally processing the hot-wire velocity data first with a detector function, which includes the slope and second derivative of velocity vs time. This function is smoothed, and then a threshold set such that if the detector function exceeds the threshold, the flow is considered turbulent. The threshold was chosen by an empirical method as a function of Reynolds number.[12] The intermittency distribution measured in a fully developed turbulent boundary layer on the NACA 0012 airfoil closely matched that found by Klebanoff.[13] A more detailed description of the intermittency calculation is found in Kerho.[12] Fluctuation spectra for the hot-wire data were not recorded. Individual hot-wire records are available upon request from the author.

Integral parameters calculated from individual velocity profiles were calculated as a measure of the development of the transition process. These parameters are formed by integrating a boundary-layer quantity at a given surface location up through the boundary layer. A useful integral quantity is obtained by integrating the turbulence intensity from the wall to 1.5δ. This technique provides a measure of the amount of turbulent kinetic energy contained in a velocity profile. It is also helpful to normalize the integrated intensity values by the airfoil chord. The equation used to calculate the normalized integrated turbulence intensity is given by

$$\hat{u}\hat{l}(x) = \frac{1}{c}\int_0^{1.5\delta} u_{rms}'(z)\,\mathrm{d}z$$

By integrating the intermittency up through the boundary layer, and nondimensionalizing by the boundary-layer thickness, the boundary-layer state can be inferred. Kerho[12] showed that this quantity is 0.0 in the laminar boundary layer and reaches a constant value of approximately 0.8 in a fully developed turbulent boundary layer. Although the use of δ as a reference length is unusual, for the case of the integrated intermittency, normalization by δ makes the intermittency profile self-similar in a fully developed turbulent boundary layer. The integrated intermittency is given by

$$\hat{\gamma}(x) = \frac{1}{\delta}\int_0^{1.5\delta} \gamma(z)\,\mathrm{d}z$$

For a typical boundary-layer velocity of 12.2 m/s, the experimental uncertainty is 1.3% in velocity and the position error less than 0.04 mm. The uncertainty in the velocity decreases substantially as the magnitude of the velocity increases. An absolute value for the experimental uncertainty in the calculation of turbulence intensity and intermittency is difficult due to the use of the digital filter and the great deal of manipulation in the case of intermittency. For turbulence intensity, the experimental uncertainty in the calculation of turbulence intensity has a maximum value of approximately 2.5% for a single measurement and 3% for the integrated value. For intermittency, when compared with a classic fully developed turbulent boundary-layer intermittency distribution observed by Klebanoff,[13] the current method of intermittency calculation yields a maximum differential of approximately 3.8%. The corresponding uncertainty in the integrated intermittency is 3.1%. Ahead of approximately $x/c = 0.07$ where the boundary layer is thin and the inviscid edge velocities high, additional errors are present. Here due to probe interference, particularly very near the model surface, errors in measured velocities may be larger. The measured turbulence intensity and intermittency in the boundary layer near the leading edge may be too large due to probe vibration. The conclusions in this paper are based on these relative measurements and not absolute measurements, which further minimizes the effects of this error. Kerho[12] presents a significantly more thorough analysis of the experimental uncertainty.

Results and Discussion

Smooth Model

Hot-wire boundary-layer measurements were first made on the smooth model to establish a baseline for comparison to the roughness data. Figure 3 shows velocity, turbulence intensity, and intermittency profiles through the boundary layer at several x/c locations at $Re = 1.25 \times 10^6$. Data were taken at x/c locations starting at the leading edge and progressing just downstream of the location where a fully developed turbulent boundary layer was measured. Measurements were taken in increments of 0.05 x/c with smaller steps taken in the transitional zone. All profiles were taken normal to the local model surface (z coordinate). The velocity profiles were observed to be laminar up to $x/c = 0.55$ with the classic linear approach to zero velocity at the wall. The profiles begin to show turbulent characteristics at $x/c = 0.60$ with fully developed turbulent profiles appearing by $x/c = 0.675$. This corresponds well to the turbulence intensity profiles, $u_{rms}'(\%)$, shown in percent of the freestream velocity. Turbulence intensity begins to grow rapidly in the boundary layer at $x/c = 0.60$ as transition begins. A maximum value of about 9% is seen in the profile at $x/c = 0.65$. By $x/c = 0.675$ this peak value is gone, and turbulent energy is moving up in the boundary layer away from the wall. Finally, note that

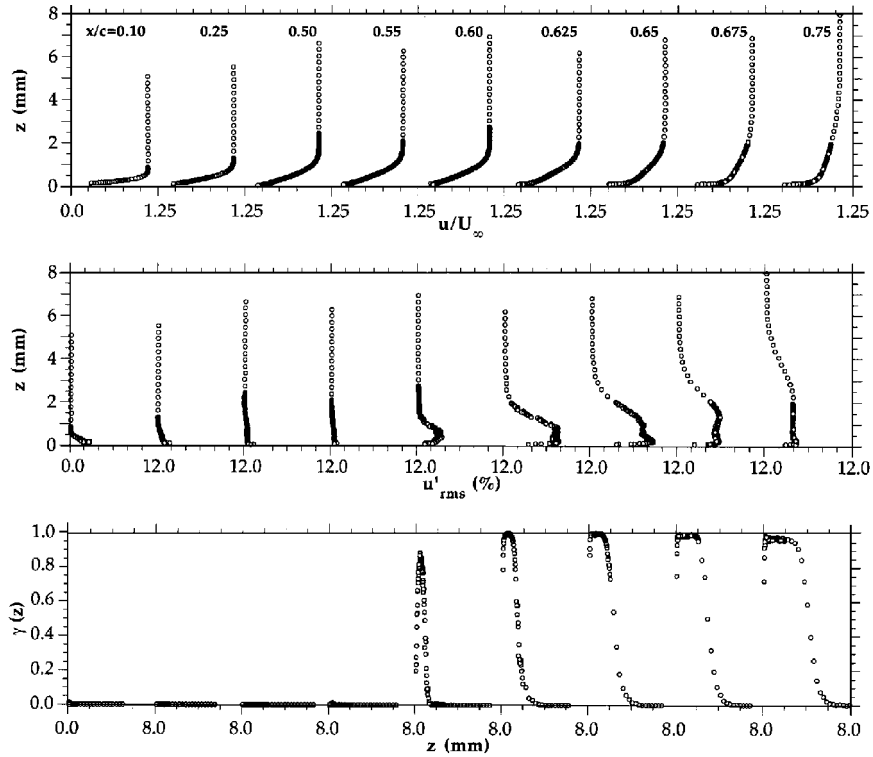

Fig. 3 Velocity, turbulence intensity, and intermittency profiles on the smooth airfoil at $Re = 1.25 \times 10^6$. Max uncertainty $u = 1.3\%$, $u'_{rms} = 2.5\%$, and $\gamma = 3.8\%$.

the intermittency is plotted γ vs z as is convention. The term γ was observed to be zero throughout the boundary layer until transition begins where intermittency spikes rapidly near the wall. As the transition process continues, γ quickly reaches a value of 1 near the wall with turbulence spreading up through the boundary layer. As the transition process is completed, the intermittency profiles attain the classic fully developed shape observed by Klebanoff.[13] Also note that as the fully turbulent boundary layer develops, γ drops toward zero near the wall. The drop toward zero in intermittency values near the wall in the fully turbulent region and the peak in the intermittency distribution in the transitional region have generally not been observed in past studies of transitional flow as reported by Owen[14] and Narasimha.[15] This drop toward zero in γ is dictated by the no-slip condition at the wall. The break toward zero in γ corresponds to the approximate height of the laminar sublayer. It is believed that the use of an insulated wall coupled with the high positional accuracy provided by the traversing system allowed the drop towards zero in γ to be observed. A more complete discussion of this effect is given by Kerho.[12]

Another beneficial means of viewing the data is through contour plots. The measurements were taken in small enough chordwise increments throughout the transitional region to allow accurate contour plots to be made of the turbulence intensity and intermittency. A gray-scale contour plot of the turbulence intensity for the smooth model at all three Reynolds numbers tested is shown in Fig. 4. In this plot the airfoil is shown in black with the contours extending up over the upper surface. The vertical scale for the boundary-layer data has been expanded by a factor of 20 in this plot to provide better visualization of the thin boundary layer. Here the TS transition process on the smooth model is seen to be a rapid and energetic process. The location of peak transition and the explosive growth of turbulence in the transitional region are clearly evident. The level of the turbulence intensity in the transition region decreases as the Reynolds number increases and the transition location moves forward toward the leading edge.

Intermittency γ contour plots are shown in Fig. 5. Here the vertical scale is normal height above the airfoil surface and has been nondimensionalized by the boundary-layer thickness δ. From Fig. 5, the intermittency is zero throughout the laminar boundary layer until the beginning of the transitional region. The constant stratified structure downstream of the initial appearance of growth in the intermittency

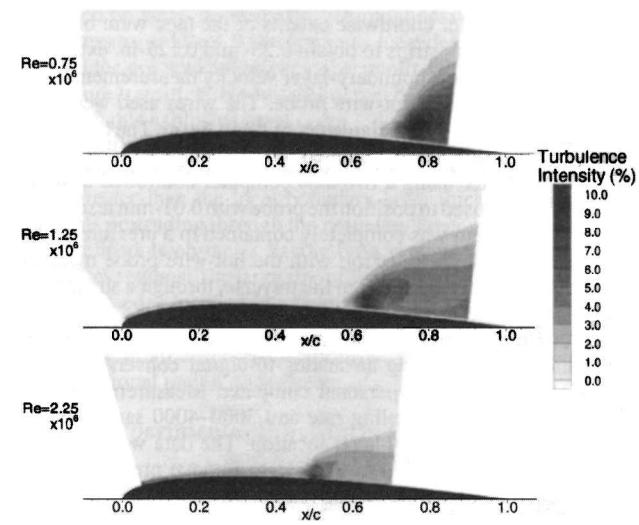

Fig. 4 Turbulence intensity contours for the smooth NACA 0012 airfoil at $\alpha = 0$ deg (vertical scale expanded by 20 times). Max uncertainty = 2.5%.

values is indicative of the fully developed turbulent boundary layer. This stratified structure is discernable as the region where the contours form bands at a relatively constant z/δ with increasing chord position. The constant stratified structure also illustrates the self-similar nature of the intermittency profile in a fully developed turbulent boundary layer when normalized by δ. The characteristic shape of the transitional region for each Reynolds number is also similar. The levels of intermittency in the stratified region compare well as a function of z/δ for all of the different Reynolds number cases. A level of intermittency greater than 0.90 occupies the region from the wall to $z/\delta \approx 0.50$. The intermittency then diffuses toward zero as the edge of the boundary layer is reached. As observed in the turbulence intensity contours, the transition region is also seen to move forward with increasing Reynolds number. For the $Re = 2.25 \times 10^6$ case, the intermittency near the wall at the leading edge is observed to be nonzero, although the boundary layer at these chord locations

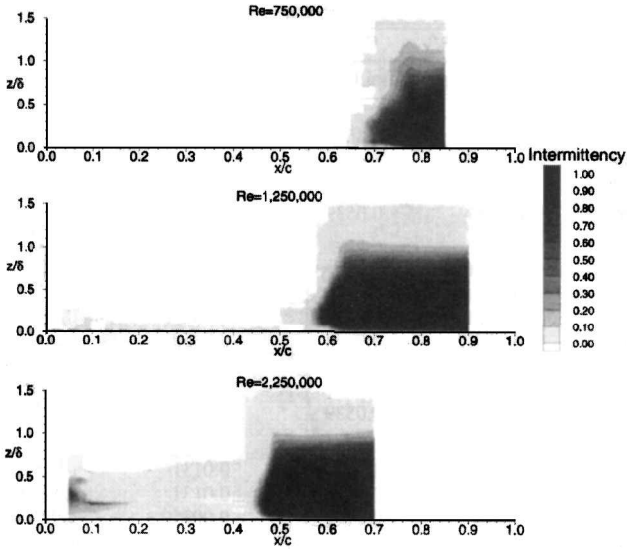

Fig. 5 Turbulent intermittency contours for the smooth model. Max uncertainty = 3.8%.

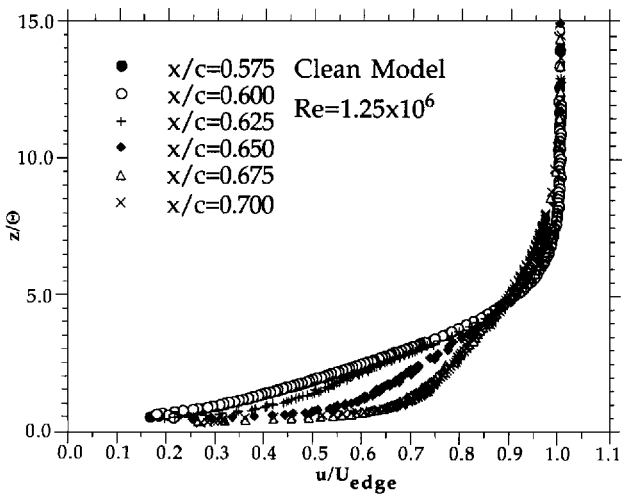

Fig. 6 Boundary-layer velocity profiles with height normalized by the momentum thickness. Max uncertainty = 1.3%.

was laminar. As discussed in the error and uncertainty analysis section, these increased intermittency values very near the leading edge are due to probe vibration.

It is also useful to have a quantitative method by which to determine when transition begins and is complete. A common method is to use the mean velocity profiles plotted with the vertical scale nondimensionalized by the boundary-layer momentum thickness θ. Velocity profiles plotted in this way are assumed to be similar in the laminar region and also similar in the turbulent region.[16] These profiles are plotted for the $Re = 1.25 \times 10^6$ case in Fig. 6. The profiles at $x/c = 0.575$ and 0.6 are clearly laminar and lie on top of each other, indicating that transition has not yet begun. The profile at $x/c = 0.625$ deviates from the laminar case, as does $x/c = 0.650$. The profiles at $x/c = 0.675$ and 0.7 are clearly turbulent and similar. Therefore, for the case of $\alpha = 0$ deg and $Re = 1.25 \times 10^6$, transition starts on the NACA 0012 airfoil between $x/c = 0.6$ and 0.625 and is complete and a fully developed turbulent velocity profile exists by $x/c = 0.65 \pm 0.675$.

A more convenient, single parameter way to do this is to plot the integrated intermittency through the boundary layer normalized by the boundary-layer thickness $\hat{\gamma}$. This is plotted for all three Reynolds numbers in Fig. 7. This method is not only more convenient but also more sensitive. The term $\hat{\gamma}$ is observed to be zero in the laminar region and quickly ramps to approximately a constant value of 0.8 in the turbulent region. The nonzero integrated intermittency observed for $Re = 2.25 \times 10^6$ at various x/c less than 10% where the

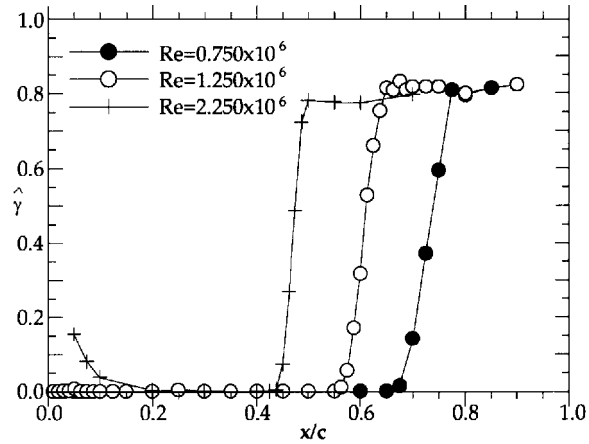

Fig. 7 Integrated intermittency vs chordwise location on the smooth model. Max uncertainty = 3.1%.

boundary layer is laminar are due to probe vibration as previously discussed. Downstream of this location, where the shear layer is much larger and boundary-layer velocities lower, the probe vibration is minimal and $\hat{\gamma}$ is zero. Noting the $Re = 1.25 \times 10^6$ case, $\hat{\gamma}$ becomes nonzero before $x/c = 0.6$ is reached and before the velocity profile could respond sufficiently to be detected in Fig. 6. Therefore, the change in $\hat{\gamma}$ as the boundary layer develops downstream will be used to determine the start and completion of the transition process. Using Fig. 7, the start and completion of boundary-layer transition is $x/c = 0.65 \pm 0.775$ for $Re = 0.75 \times 10^6$, $x/c = 0.575 \pm 0.675$ for $Re = 1.25 \times 10^6$, and $x/c = 0.4375 \pm 0.50$ at $Re = 2.25 \times 10^6$. These results show that transition occurs earlier and over a shorter distance as the Reynolds number is increased. These transition locations compare reasonably well to those determined from surface oil flow visualization,[10] $x/c = 0.72$, 0.61, and 0.49 at $Re = 0.75$, 1.25, and 2.25×10^6, respectively. However, the completion of transition as determined from Fig. 7 is downstream of these locations because the oil flow senses only when the surface shear exceeds the value needed for the oil to flow and not the development of the entire boundary layer. Surface oil flow visualization was also performed to confirm the two-dimensionality of the smooth case transition front. The front proved to be very two dimensional, and these results are reported in detail by Bragg et al.[10]

Roughness Effects

Detailed boundary-layer measurements were made using several different distributed roughness extents and leading-edge locations. Chordwise extent of the roughness was varied from $\frac{1}{8}$ to $\frac{1}{2}$ in. The chordwise placement of the roughness was measured in surface length from the stagnation point ($x/c = 0$ and $y/c = 0$) to the leading edge of the roughness strip and varied from $s = 4$ to 24 mm. The test matrix of chordwise extents and placements provided for a range of roughness k/δ from 0.51 to 2.5, depending upon test Reynolds number. The roughness Reynolds numbers Re_k varied from 395 at the lower Reynolds number, 0.75×10^6, up to 1582 at the highest Reynolds number, 2.25×10^6. Complete sets of boundary-layer measurements were made for each individual case at x/c locations directly behind the roughness progressing downstream to the point where a fully developed boundary layer was measured. On average 18–25 profiles were taken for each case. For the purpose of this discussion, only a subset of the overall test matrix will be reported in detail. The results presented provide the general trend for all roughness measurements obtained. A summary of the entire test matrix will be provided at the end of this discussion.

For all roughness cases in this investigation calculations were performed to determine the critical distributed roughness height required to cause transition based upon the empirical formulations of Braslow et al.[9] The critical roughness heights were calculated to provide a basic means of general comparison with other distributed roughness results. The ISES[17] airfoil aerodynamic analysis and design code was used to provide the undisturbed smooth model boundary-layer parameters for these calculations. All roughness leading- and trailing-edge Re_k, k/δ, x/c, and s/c locations are

Table 1 Roughness extent and location data

Roughness cases	Re_k		k/d		x/c		s/c	
	Leading edge	Trailing edge	Leading edge	Trailing edge	Leading edge	Trailing edge	Leading edge	Trailing edge
$Re = 0.75 \times 10^6$								
1/8 in. at 7 mm	395	459	1.22	1.03	0.00490	0.000910	0.0131	0.0191
1/4 in. at 7 mm	395	499	1.22	0.897	0.00490	0.0138	0.0131	0.0250
1/2 in. at 4 mm	287	522	1.43	0.814	0.00187	0.0191	0.00750	0.0313
1/2 in. at 24 mm	523	479	0.656	0.506	0.0314	0.0539	0.0450	0.0688
$Re = 1.25 \times 10^6$								
1/8 in. at 7 mm	656	766	1.57	1.34	0.00490	0.00910	0.0131	0.0191
1/4 in. at 7 mm	656	834	1.57	1.16	0.00490	0.0138	0.0131	0.0250
1/2 in. at 4 mm	479	878	1.84	1.05	0.00187	0.0191	0.00750	0.0313
1/2 in. at 8 mm	701	907	1.50	0.925	0.00612	0.0258	0.0150	0.0388
1/2 in. at 12 mm	811	920	1.22	0.833	0.0117	0.0327	0.0225	0.0463
1/2 in. at 18 mm	899	918	1.01	0.732	0.0212	0.0432	0.0337	0.0575
1/2 in. at 24 mm	919	899	0.848	0.655	0.0314	0.0539	0.0450	0.0688
$Re = 2.25 \times 10^6$								
1/8 in. at 7 mm	1182	1378	2.14	1.81	0.00490	0.00910	0.0131	0.0191
1/4 in. at 7 mm	1182	1502	2.14	1.57	0.00490	0.0138	0.0131	0.0250
1/2 in. at 4 mm	854	1582	2.50	1.42	0.00187	0.0191	0.00750	0.0313

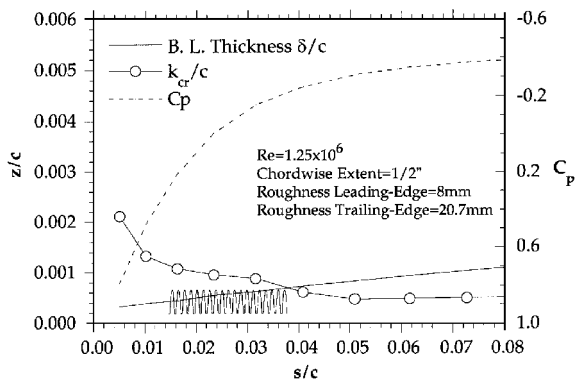

Fig. 8 Plot of critical roughness height compared with boundary-layer thickness and actual roughness location and height with the local pressure distribution also included.

given in Table 1 as a function of test Reynolds number. The individual roughness cases are classified by the roughness chordwise extent in inches and the surface length from the model stagnation point ($x/c = 0$ and $y/c = 0$) to the leading edge of the roughness in millimeters. By definition, Re_k and k/δ values are based upon the smooth model flowfield; due to the high density of the distributed roughness and the substrate thickness, blockage effects will cause the boundary layer to be displaced outward, increasing δ in the actual roughness induced boundary layer.

Figure 8 shows the critical roughness height calculations performed for a distributed roughness distribution at $Re = 1.25 \times 10^6$. The roughness is $\frac{1}{2}$ in. in the chordwise direction with the leading edge of the roughness 8 mm in surface length aft of the stagnation point (leading edge) and the trailing edge of the roughness at 20.7 mm. For this Reynolds number and roughness placement, Re_k varied from 701 to 907 depending upon chordwise location over the roughness. Figure 8 also shows the roughness plotted with respect to the undisturbed boundary-layer thickness predicted by ISES. Note that the roughness shape is distorted because the plot aspect ratio is not 1. The height that the base of the roughness is displaced up off the surface in Fig. 8 is equal to the height of the tape substrate. Also included in Fig. 8 is the local pressure distribution plotted on the opposite axis showing the magnitude of the pressure gradient. From Fig. 8, the leading edge of the roughness is seen to be at a height greater than the undisturbed boundary-layer thickness, whereas the trailing-edge height is slightly submerged. Because of the low Re_x values at this location, the $Re_{k,\,\mathrm{crit}}$ values obtained from Braslow et al.[9] are large, approximately 1200. As a result, the critical height at these low Re_x values is also large due to the high $Re_{k,\,\mathrm{crit}}$ values coupled with the low edge velocities encountered in the stagnation region. For this case, the roughness height is well below that required for transition to occur at the roughness as predicted by Braslow et al. over most of the extent of the roughness. Although still below the predicted critical height, the trailing edge of the roughness does approach the critical value.

Figure 9 shows the velocity, turbulence intensity, and intermittency profiles for this distributed roughness case at $Re = 1.25 \times 10^6$. The first velocity profile shown at $x/c = 0.05$ is already transitional and has high shear near the wall. Note that the aft edge of the roughness was at $x/c = 0.0258$. The velocity profiles develop very slowly with increasing chordwise position. From the mean velocity profiles alone, one might assume the boundary layer to be fully transitioned. The corresponding turbulence intensity values are much lower than those observed on the smooth model during transition. The largest values measured behind the roughness in Fig. 9 are approximately 4%. For the smooth model at $Re = 1.25 \times 10^6$, values greater than 9% are seen during transition. As compared with the smooth model natural transition process, the roughness induced transition is not very energetic in u'_{rms}. Since v' and w' fluctuating velocities were not obtained, it is uncertain whether the roughness induced transition is less energetic overall than the smooth model case. From the turbulence intensity data alone, it is also unclear where the transition process is complete.

Although the mean velocity profiles exhibit a characteristic turbulent shape at $x/c = 0.05$, the intermittency distributions do not show a fully developed turbulent character until an $x/c \approx 0.40$. For the first profile at $x/c = 0.05$, the intermittency reaches a value near 0.75; however, the intermittency profile grows very slowly and does not reach a maximum value near the wall until $x/c = 0.30$ and does not have fully developed turbulent boundary-layer characteristics until $x/c = 0.40$.

Figure 10 shows a contour plot of the turbulence intensity for the smooth and distributed roughness case. The distributed roughness case shows a completely different character from that observed for the smooth model. No hot spot in the streamwise turbulence intensity denoting a peak transition location is observed. The maximum streamwise turbulence intensity levels are significantly lower. Transition due to the distributed roughness is being accomplished through a completely different mechanism than that observed for the smooth model. The intensity increases up from the surface as the boundary layer grows downstream and intensity values grow slowly with increasing chord position. Again, as discussed earlier, these measurements represent streamwise fluctuating velocities only.

Contours of intermittency for the roughness and for the smooth model are shown in Fig. 11. The roughness case shows a slow asymptotic growth from the roughness location to a point downstream where the constant stratified structure indicative of the fully developed turbulent boundary layer is evident. Intermittency values near the wall behind the roughness grow quickly to values on the order of 0.90 but require more time to spread upward throughout the boundary layer. Once the constant stratified structure is obtained,

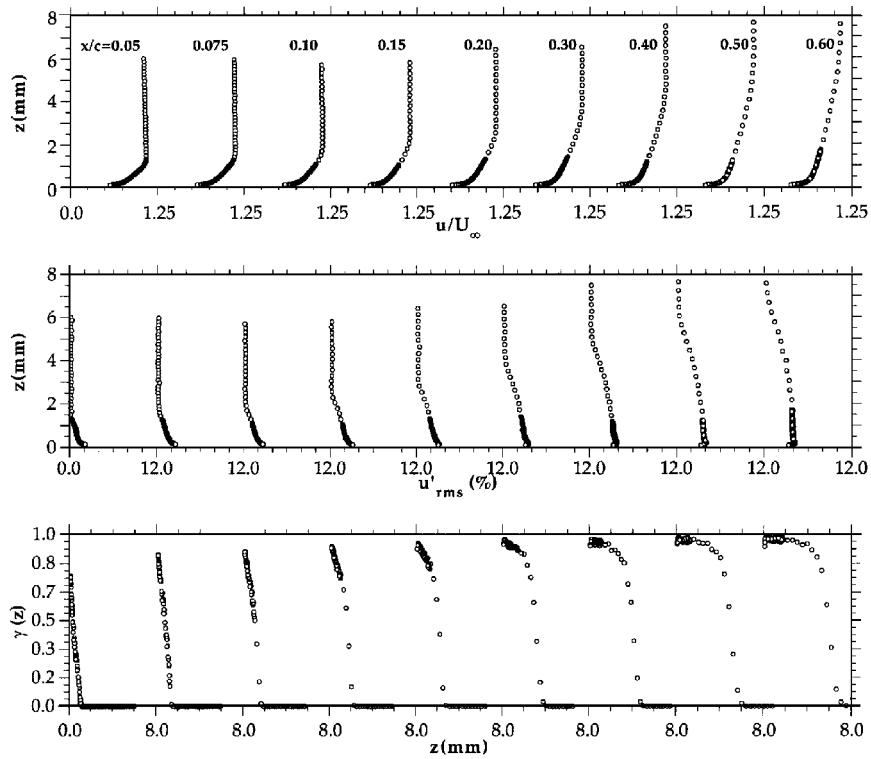

Fig. 9 Velocity, turbulence intensity, and intermittency on the airfoil at $Re = 1.25 \times 10^6$ with $\frac{1}{2}$ chordwise roughness starting at $s = 8$ mm. Max uncertainty $u = 1.3\%$, $u'_{rms} = 2.5\%$, and $\gamma = 3.8\%$.

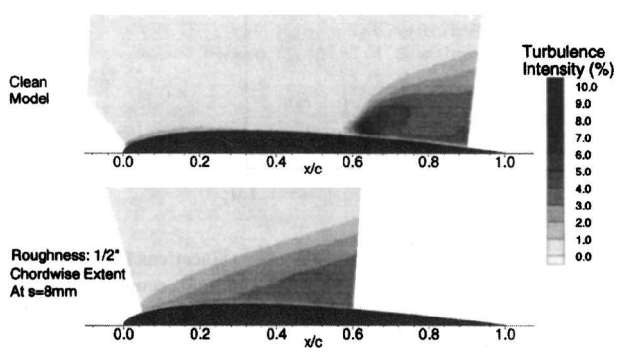

Fig. 10 Turbulence intensity contours for the smooth model and the model with $\frac{1}{2}$-in. chordwise roughness extent starting at $s = 8$ mm for $Re = 1.25 \times 10^6$ (vertical scale expanded by 20 times). Max uncertainty = 2.5%.

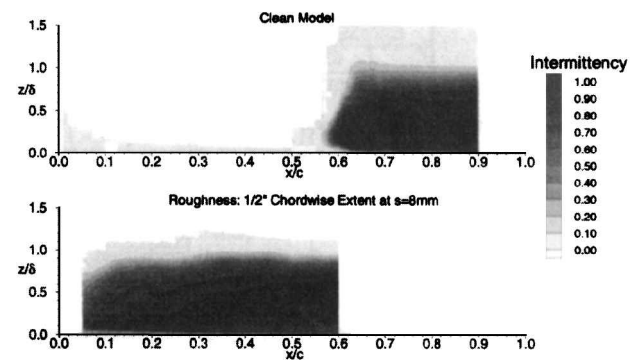

Fig. 11 Intermittency contours for the smooth model and the model with $\frac{1}{2}$-in. chordwise roughness extent starting at $s = 8$ mm for $Re = 1.25 \times 10^6$. Max uncertainty = 3.8%.

the character of this structure is relatively equivalent to the smooth case.

The integrated turbulence intensity and intermittency are shown in Figs. 12 and 13 for the smooth model and the model with five roughness cases, including the roughness simulation reported in Figs. 9–11. The chordwise extents of the roughness are $\frac{1}{2}$ in. with various placements from $s = 4$ to 24 mm at $Re = 1.25 \times 10^6$. Figure 12 shows the integrated turbulence intensity $\hat{u}\prime$. For the smooth model, the integrated intensity remains at a constant near zero throughout the laminar boundary layer ($x/c = 0.01$–0.5625) and ramps up steeply as the transitional region is encountered. The sharp growth in $\hat{u}\prime$ subsides around $x/c = 0.6625$, where a definitive peak is observed. The x/c location of this peak corresponds to the hot spot observed in the turbulence intensity contour shown in Figs. 4 and 10. The integrated intensity values are seen to decrease slightly past this peak before continuing to grow. The roughness induced boundary layer, however, shows a completely different result. The integrated turbulence intensity is seen to grow almost linearly beginning directly downstream of the roughness. This type of growth does not imply transition due to a primary TS mechanism as observed for the smooth model. All roughness cases appear to initiate the transition process directly downstream of the roughness. For the long roughness chordwise extent of $\frac{1}{2}$ in. the location of the roughness for these cases appears to have little effect upon the onset of transition. The $\hat{u}\prime$ values grow linearly with chord position. The slope of these curves is essentially the same. Only the case at $s = 4$ mm is unique in that the curve is slightly shifted to the right, although the slope is equivalent to the other cases. The small shift to the right implies a slightly delayed transition onset (1–2% chord). Since u'_{rms} measured at a point in the boundary layer is related to the turbulent kinetic energy, the integrated value is an indication of the total streamwise turbulent energy in the boundary layer. The rough cases all show a much slower growth rate of the streamwise turbulent energy than that experienced in the smooth case during transition. Measurements of $v\prime$ and $w\prime$ would be useful to determine whether the turbulent energy has been transferred from $u\prime$ to other modes.

Figure 13 shows the integrated intermittency values normalized by local boundary-layer thickness for the smooth model and model with roughness at $Re = 1.25 \times 10^6$. From Fig. 13, the roughness integrated intermittency values grow rapidly downstream of the roughness and then asymptotically approach the fully developed turbulent state similar to that observed for the smooth model. None of the $\frac{1}{2}$-in. roughness cases shown in Fig. 13 appear to exhibit the primary

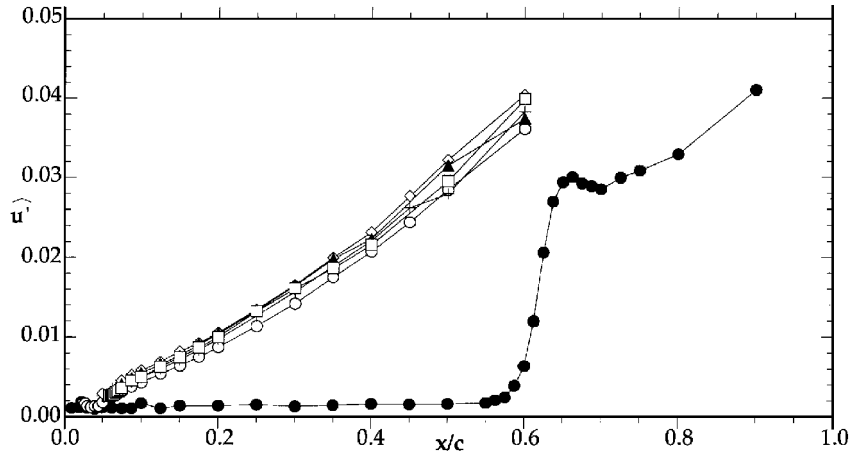

Fig. 12 Integrated turbulence intensity for the smooth model and the model with $\frac{1}{2}$-in. chordwise extent of roughness at several locations from $s = 4$ to 24 mm for $Re = 1.25 \times 10^6$. Max uncertainty = 3.0%: ● clean model; ○ roughness at $s = 4$ mm; +, roughness at $s = 8$ mm; ◇ roughness at $s = 12$ mm; ▲, roughness at $s = 18$ mm; and □, roughness at $s = 24$ mm.

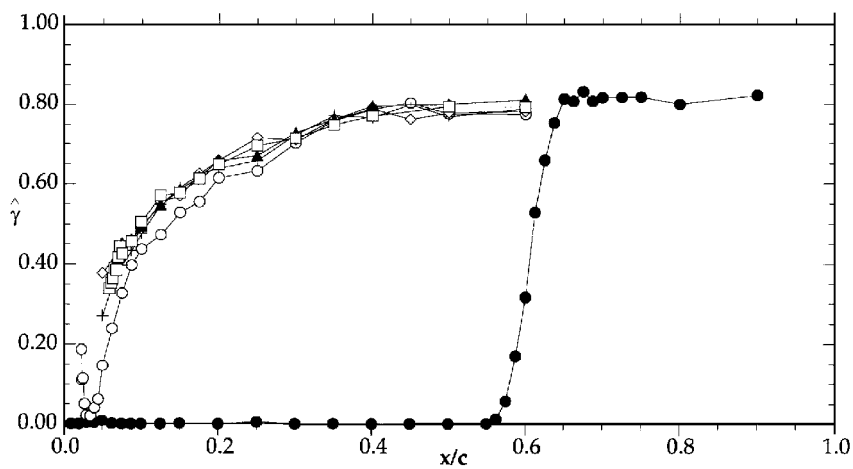

Fig. 13 Integrated intermittency for the smooth model and the model with $\frac{1}{2}$-in. chordwise extent of roughness at several locations from $s = 4$ to 24 mm for $Re = 1.25 \times 10^6$. Max uncertainty = 3.1%: ● clean model; ○ roughness at $s = 4$ mm; +, roughness at $s = 8$ mm; ◇ roughness at $s = 12$ mm; ▲, roughness at $s = 18$ mm; and □, roughness at $s = 24$ mm.

instability TS type breakdown observed for the smooth model. As seen in the integrated streamwise turbulence intensities in Fig. 12, the transition process is initiated at or very near the roughness trailing edge but requires a substantial chordwise extent to reach a fully developed turbulent boundary layer. Although the initial growth in $\hat{\gamma}$ is on the order of the initial growth for the smooth model the last rise from $\hat{\gamma} \approx 0.60$ to 0.80 is slow and requires a substantial chordwise extent. The length of the transitional region appears to be roughly equivalent for all the cases shown, $\Delta x_{tr}/c \approx 0.40$, with the exception that the $s = 4$ mm case is slightly smaller at $\Delta x_{tr}/c \approx 0.38$.

Unlike the other methods presented for viewing and analyzing the data, the integrated intermittency provides a clear and distinct means of determining the beginning and end of the transitional zone. For his study of the flowfield resulting from a single isolated hemisphere on a flat plate with zero pressure gradient, Klebanoff et al.[18] chose to look for similarity in his measured mean velocity profile with that for a fully developed smooth plate turbulent profile. Like the results obtained from the distributed roughness tested in this study, Klebanoff also found that the transitional intermittency behind the single element produced relatively high values near the wall but required a substantial distance to diffuse up through the whole boundary layer. A study by Klebanoff and Diehl,[19] however, found that the boundary layer retains a long memory of disturbances introduced by obstacles. It therefore might not be reasonable to assume that a roughness induced turbulent boundary layer should ever exhibit total similarity with a TS induced turbulent boundary layer. The study by Dhawan and Narasimha[16] found that a fully developed turbulent boundary layer will exhibit similarity when normalized by momentum thickness. As a result, it might be reasonable to assume that a fully developed roughness induced turbulent boundary layer might exhibit this same type of similarity with itself.

As was done for the smooth model in Fig. 6 the mean velocity profiles for a roughness induced boundary layer were normalized by momentum thickness and plotted. Figure 14 shows a plot of several mean velocity profiles normalized by momentum thickness through the transitional region for the case of $\frac{1}{2}$-in. roughness at $s = 8$ mm and $Re = 1.25 \times 10^6$. The analysis for this roughness case was presented in Figs. 9–13. From Fig. 14, the normalized velocity profiles begin to show similarity at an $x/c = 0.30$. Beyond this point, the profiles slowly become more similar with increasing x/c. The integrated intermittency for the case of $\frac{1}{2}$-in. roughness at $s = 8$ mm and $Re = 1.25 \times 10^6$ was shown in Fig. 13. From Fig. 13, beyond $x/c = 0.30$, the integrated intermittency has reached a value of 0.70 and is asymptotically approaching the fully developed value of ≈ 0.80 at $x/c = 0.40$. This result compares well with the mean velocity profile similarity shown in Fig. 13. As a result, it can be concluded that the use of the intermittency profile to determine the chordwise location where a fully developed turbulent boundary layer exists is both reasonable and accurate for the roughness induced boundary layers encountered in this investigation.

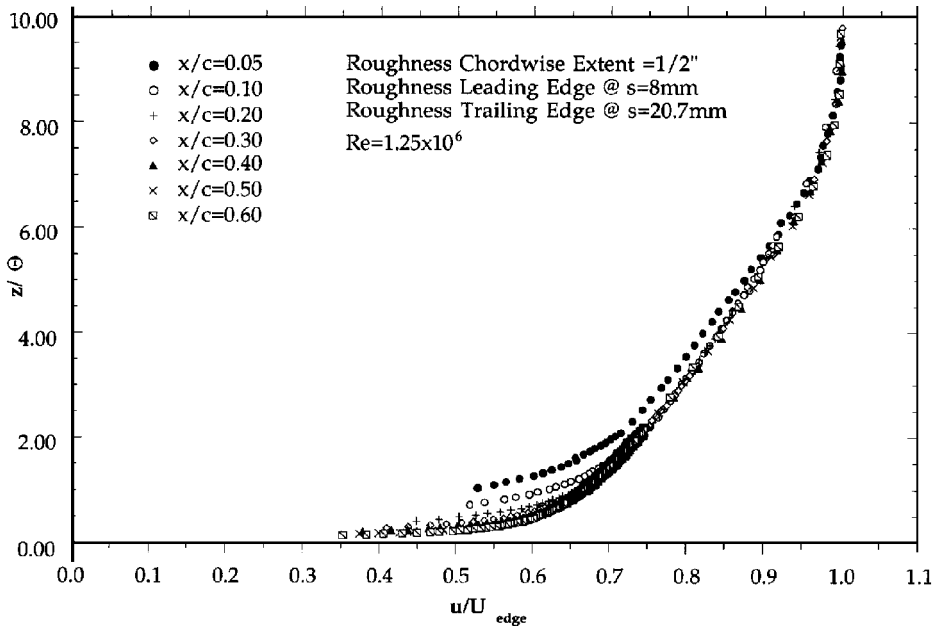

Fig. 14 Boundary-layer velocity profiles with height nondimensionalized by momentum thickness for $\frac{1}{2}$-in. chordwise roughness extent starting at $s = 8$ mm for $Re = 1.25 \times 10^6$.

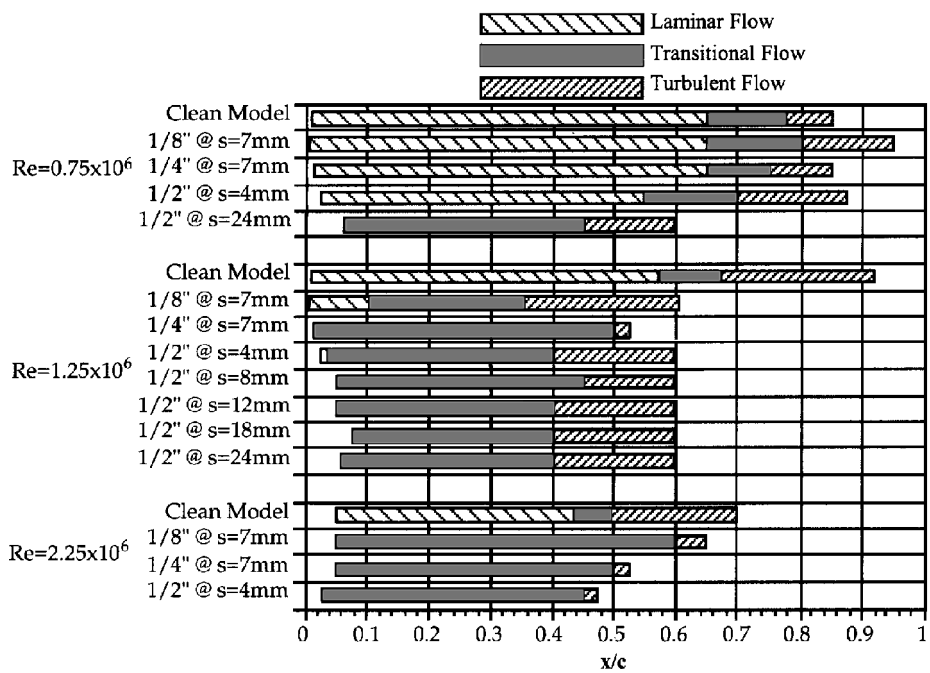

Fig. 15 Boundary-layer states for the smooth model and all distributed roughness cases tested as a function of Reynolds number. Max uncertainty is between 2.5 and 5%, depending upon chord position.

From the integrated intermittency results, regions of laminar, transitional, and turbulent flow were determined and compiled for the smooth model and all roughness cases studied. Figure 15 shows the compiled chordwise length and location of the transitional region for the entire test matrix. Cases are grouped by Reynolds number and identified by the chordwise extent of the roughness and the suface length from the stagnation point to the leading edge of the roughness. The error in determining the length and location of the transitional region from the plots of $\hat{\gamma}/\delta$ is dependent upon the density of chordwise measurement locations through this region. On average, the error is approximately 2.5%, but it can be as large as 5% for a few cases. From Fig. 15, the extent of the transitional region is seen to decrease with increasing Reynolds number for the smooth model from $\Delta x_{tr}/c = 0.125$ at $Re = 0.75 \times 10^6$ to $\Delta x_{tr}/c = 0.10$ at $Re = 1.25 \times 10^6$ to $\Delta x_{tr}/c = 0.0625$ at $Re = 2.25 \times 10^6$. The extent of the $\frac{1}{2}$-in. roughness induced transitional regions was fairly consistent with an average value of $\Delta x_{tr}/c = 0.37$ regardless of Reynolds number or location. The extent of the $\frac{1}{4}$-in. roughness induced transitional regions also appeared to be fairly consistent with an average value of $\Delta x_{tr}/c = 0.47$. Only the cases for $Re = 2.25 \times 10^6$ were shown to produce a roughness induced transitional region for all three roughness extents tested. From Fig. 15, the extent of the transitional region at $Re = 2.25 \times 10^6$ decreases with increasing roughness extent. For the $\frac{1}{8}$-, $\frac{1}{4}$-, and $\frac{1}{2}$-in. roughness extents, $\Delta x_{tr}/c = 0.55$, 0.45, and 0.425, respectively. In general, the extent of the transitional region appears to be fairly consistent for an individual roughness extent and not strongly dependent upon location or Reynolds number. The results for the $\frac{1}{8}$-in. roughness

at $s = 7$ mm and $Re = 1.25 \times 10^6$ do not agree with this trend because the transition process was observed to be a result of some type of vortex shedding breakdown and not the typical roughness induced transitional process.[12] The length of the transitional region also appears to decrease with increasing roughness extent. It is also clear from Fig. 15 that the extent of the transitional region is substantially greater for the roughness induced boundary layer than for the smooth transition process.

Summary and Conclusions

An experimental study of the effects of large distributed roughness located near the leading edge of an airfoil has been performed to determine the effect on boundary-layer development and transition. The effects of the large distributed roughness on the boundary-layer development and transitional region were markedly different from the smooth model transitional process. This implies that the roughness induced transition process was governed by completely different mechanisms than those present in the natural transition process documented for the smooth model. In general, the roughness was observed to trigger the transition process at, or very near, the trailing edge of the roughness. The ensuing transitional boundary layer required a substantial chordwise extent (at least 30% chord) to reach a fully developed turbulent state. A fully turbulent boundary layer was never observed to occur at the roughness location. Roughness below a critical Re_k value was observed to either have no effect upon transition or to promote early transition downstream of the roughness in a manner similar to that observed on the smooth model (some $Re = 0.75 \times 10^6$ cases; see Fig. 15). Transition was not observed to be a switch. A finite distance was required for the transitional process for both the roughness induced and smooth model transition.

The extended transitional region observed for the roughness used in this investigation does not generally conform to the definitions and results of distributed roughness critical Re_k studies discussed in the literature or observed by other researchers. By definition, the critical roughness Reynolds number is that set of flow conditions under which transition will occur at the roughness element or location. The problem with the definition of $Re_{k,\,\mathrm{crit}}$ is that the statement, "transition occurs at the roughness element or location" is vague. What is meant by the word transition and how it was measured varies from researcher to researcher. As a result, the means by which individual researchers define transition at the roughness element or at the location of the roughness varies widely. The purpose of this study was to document the development of the boundary layer as a result of the presence of large distributed roughness and not to perform an $Re_{k,\,\mathrm{crit}}$ study. A detailed $Re_{k,\,\mathrm{crit}}$ study with the very large and densely packed roughness used in this investigation located in the leading-edge region of an airfoil would prove interesting and provide a valuable data set.

The low turbulence intensity values of the roughness induced boundary layer are surprising. Transition due to distributed roughness is commonly described as explosive because there is no slow buildup of an instability leading to an initial breakdown and appearance of turbulent spots. Results from this investigation show that after breakdown has begun, the smooth model transition process is more aptly termed explosive than the transition process induced by the distributed roughness. The smooth model natural transition process repeatedly produced streamwise turbulent energy levels twice as high as those observed for the roughness induced boundary layer. The length of the transitional region was much shorter for the smooth model transition process. The roughness induced transitional region possessed no discernable peak transition location. Intermittency values very near the wall ($z/\delta < 0.2$) directly downstream of the roughness were seen to grow quickly to levels denoting locally turbulent flow. The distribution of intermittency up through the boundary-layer profile at that given x/c location was, however, by no means fully developed. A substantial chordwise extent was required for these high intermittency levels to migrate up through the boundary layer.

In general, the chordwise extent of the transitional region appeared to be fairly consistent for an individual roughness extent and relatively insensitive to location or Reynolds number over the relatively small range tested. The length of the transitional region was also shown to decrease with increasing roughness extent. The larger the relative height of the roughness to the boundary-layer thickness and the longer its chordwise extent, the more likely the roughness was to trigger the transition process.

Results from this investigation have important implications to the proper modeling of the ice accretion process. Results have shown that although distributed roughness typical of that present during the accretion process generally triggers the transition process, the resulting transitional boundary layer does not reach a fully developed turbulent state immediately as previously assumed. This result has broad implications in the development of a more accurate ice accretion model.

Acknowledgments

The work was funded under NASA Grant NAG 3-1134. The authors would like to thank Matt Cummings for his assistance and contributions on this project. The authors would also like to thank Jaiwon Shin of the NASA Lewis Research Center for his significant contributions to this research.

References

[1]Gregory, N., and Walker, W. S., "The Effects of Transition of Isolated Surface Excrescences in the Boundary-Layer," Aeronautical Research Council, Repts. and Memoranda 2779, London, Oct. 1951.

[2]Acarlar, M. S., and Smith, C. R., "A Study of Hairpin Vortices in a Laminar Boundary Layer. Part 1. Hairpin Vortices Generated by a Hemisphere Protuberance," *Journal of Fluid Mechanics*, Vol. 175, Feb. 1987, pp. 1–41.

[3]Morkovin, M. V., "Bypass Transition to Turbulence and Research Desiderata," NASA-CP-2386, May 1984, pp. 161–204.

[4]Kendall, J. M., "The Effect of Small-Scale Roughness on the Mean Flow Profile of a Laminar Boundary Layer," *Instability and Transition*, edited by M. Y. Hussaini and R. G. Voigt, Vol. 1, Springer–Verlag, New York, 1990, pp. 296–302.

[5]Corke, T. C., Bar-Sever, A., and Morkovin, M. V., "Experiments On Transition Enhancement by Distributed Roughness," *Physics of Fluids*, Vol. 29, No. 10, 1986, pp. 3199–3213.

[6]Tadjfar, M., Reshotko, E., Dybbs, A., and Edwards, R. V., "Velocity Measurements Within Boundary Layer Roughness Using Index Matching," Fluids Engineering Div., American Society of Mechanical Engineers, FED Publication 33, New York, Nov. 1985.

[7]Tani, I., "Effect of Two-Dimensional and Isolated Roughness on Laminar Flow," *Boundary Layer and Flow Control, Volume 2*,,edited by G. V. Lachmann, Pergamon, Oxford, England, UK, 1961, pp. 637–656.

[8]Von Deonhoff, A. E., and Braslow, A. L., "The Effect of Distributed Surface Roughness on Laminar Flow," *Boundary Layer and Flow Control, Volume 2*,edited by G. V. Lachmann, Pergamon, Oxford, England, UK, 1961, pp. 657–681.

[9]Braslow, A. L., Hicks, R. M., and Harris, R. V., "Use of Grit-Type Boundary-Layer Transition Trips on Wind-Tunnel Models," NASA TN D-3579, Sept. 1966.

[10]Bragg, M. B., Kerho, M. F., and Cummings, M. J., "Effect of Ice Roughness on Airfoil Aerodynamics," AIAA Paper 94-0800, Jan. 1994.

[11]Norman, R. S., "On Obstacle Generated Secondary Flows in Laminar Boundary-Layers and Transition to Turbulence," Ph.D. Thesis, Dept. of Mechanical Engineering, Illinois Inst. of Technology, Chicago, IL, 1972.

[12]Kerho, M. F., "Effect of Large Distributed Roughness Near an Airfoil Leading Edge on Boundary-Layer Development and Transition," Ph.D. Dissertation, Dept. of Aeronautical and Astronautical Engineering, Univ. of Illinois at Urbana–Champaign, Urbana, IL, 1995.

[13]Klebanoff, P. S., "Characteristics of Turbulence in a Boundary-Layer with Zero Pressure Gradient," NACA Rept. 1247, 1955.

[14]Owen, F. K., "Transition Experiments on a Flat Plate at Subsonic and Supersonic Speeds," *AIAA Journal*, Vol. 8, No. 3, 1970, pp. 513–523.

[15]Narasimha, R., "The Laminar-Turbulent Transition Zone in the Boundary-Layer," *Progress in Aerospace Sciences*, Vol. 22, Pergamon, Oxford, England, UK, 1985, pp. 29–80.

[16]Dhawan, S., and Narasimha, R., "Some Properties of Boundary Layer Flow During the Transition from Laminar to Turbulent Motion," *Journal of Fluid Mechanics*, Vol. 3, Pt. 4, Jan. 1958, pp. 418–436.

[17]Drela, M., and Giles, M., "A Users Guide to ISES," Computational Aerospace Sciences Lab., Massachusetts Inst. of Technology, Cambridge, MA, Aug. 1989.

[18]Klebanoff, P. S., Cleveland, W. G., and Tidstrom, K. D., "On the Evolution of a Turbulent Boundary-Layer Induced by a Three-Dimensional Roughness Element," *Journal of Fluid Mechanics*, Vol. 237, April 1992, pp. 101–187.

[19]Klebanoff, P. S., and Diehl, Z. W., "Some Features of Artificially Thickened Turbulent Boundary-Layers," NACA TN 2475, Oct. 1951.